Journal of Intelligent Material Systems and Structures

Acoustic Measurements Using a Fiber Optic Sensor System

Miao Yu and B. Balachandran

The online version of this article can be found at:

Additional services and information for *Journal of Intelligent Material Systems and Structures* can be found at:

Email Alerts: http://jim.sagepub.com/cgi/alerts

Subscriptions: http://jim.sagepub.com/subscriptions

Reprints: http://www.sagepub.com/journalsReprints.nav

Permissions: http://www.sagepub.co.uk/journalsPermissions.nav

Citations http://jim.sagepub.com/cgi/content/refs/14/7/409

Acoustic Measurements Using a Fiber Optic Sensor System

MIAO YU[1] AND B. BALACHANDRAN[2],*

[1]*Intelligent Optics Laboratory, Institute for Systems Research, University of Maryland, College Park, Maryland 20742, USA*

[2]*Department of Mechanical Engineering, University of Maryland, College Park, Maryland 20742, USA*

ABSTRACT: Recent work conducted on developing a fiber tip based Fabry-Perot (FTFP) sensor system for acoustic measurements is presented in this article. It has been determined that this system can be used to detect acoustic fields in the frequency range of 20 Hz–6 kHz with an optical phase sensitivity of 0.095 rad/Pa. A series of experiments is performed to investigate the possibility and potential use of this sensor system, which is designed to be implemented in a multiplexed architecture for providing response measurements to a structural acoustic control system.

Key Words: fiber optic sensor, Fabry-Perot, acoustic measurements

INTRODUCTION

ACOUSTIC pressure measurements are needed in many applications ranging from flow control over underwater vehicles to vibration and noise control problems in transport vehicles. In the design of modern transportation vehicles, structural vibration and interior noise have become important problems that need to be addressed. For example, in helicopter systems, control of noise transmission into enclosed spaces is an important problem. This noise transmission can be classified into structure-borne noise transmission and air-borne noise transmission. While the former is associated with energy transmitted through the fuselage into the cabin, the latter is associated with energy transmitted through air into the cabin. Various studies have shown that the predominant frequency components associated with the noise transmission lie in the frequency range of 50–5500 Hz (e.g., Nashif et al., 1985). There are various approaches that can be used to control sound fields inside a helicopter cabin (e.g., Nelson and Elliott, 1994; Balachandran et al., 1996; Fuller et al., 1996). An integral part of these approaches is the sensor system. Among the different approaches, one of the approaches is based on controlling the radiation (transmission) from (through) a flexible structure by active means. For this approach, which is referred as active structural acoustics control (ASAC), the following components are important: (a) sensors (error measurements and reference measurements), (b) actuators, and (c) control scheme. The present efforts are being pursued with the goal of developing a distributed sensor array for

control of sound fields inside enclosures and sound radiation from flexible structures.

Fiber optic sensors have the advantages of being light weight, having high sensitivity, and easy multiplexibility. Since the original demonstrations showed that optical fibers could be utilized as acoustic sensors (Bucaro et al., 1977; Cole et al., 1977), substantial research work has been done in this field. Most of these efforts have been directed towards development of hydrophones for ultrasonic detection (Li and Zhang, 1998; Koch, 1999; Beard et al., 2000). Among those sensors, it has been shown that Bragg grating sensors can be easily multiplexed by using wavelength division multiplexing (WDM) techniques. However, the limited sensor bandwidth associated with such systems is an issue that needs to be addressed. In addition, low sensitivity due to the high Young's modulus of silica results in "small" acoustically induced strains, which also limits the application of these types of sensors (Baldwin et al., 1999; Takahashi et al., 2000). Hence, low-finesse Fabry-Perot (FP) sensors have become attractive choices for a high-performance sensing in this area (He and Cuomo, 1992; Zhou et al., 1995). In such cases, a FP cavity formed between the fiber tip and the object surface is a clear solution. There are two types of modulation schemes used to recover the signal, one being intensity modulation schemes and the other being phase modulation schemes. Intensity modulated sensors offer simplicity of design and ease of implementation, but they suffer from problems of limited sensitivity, low dynamic range, and drift due to intensity fluctuation. Phase modulated sensors are based on detection of the acoustically induced optical phase shift by using an interference technique. They have high sensitivity and do not suffer from optical source and receiver drift

*Author to whom correspondence should be addressed.
E-mail: balab@glue.umd.edu

problems, but their nonlinear input–output characteristics require careful design of the demodulation scheme.

In this paper, a novel fiber tip based Fabry-Perot (FTFP) sensor system is developed for acoustic pressure measurements in the range of 20 Hz–6 kHz, the typical range of interest for helicopter systems. The demodulation scheme of this sensor system falls in the category of phase modulation schemes discussed above, and this system is designed to work in an acoustic control system with multiple sensor inputs. A digital phase demodulation system based on a phase-stepping technique has been developed for this sensor system to decode the optical intensity signal into optical phase signal. The experimental results demonstrate the feasibility of using such a sensor system to detect acoustic signals. Details of the sensor modeling and design are discussed. The experimental arrangement and the experimental results are presented and discussed as well.

MODEL DEVELOPMENT

In this section, the interferometers comprising the optical system and the mechanical component response are discussed.

Optical System

The sensing system under investigation is based on a low-finesse FP cavity. As shown in Figure 1 (a), after the light emerges from the single mode fiber, the electric field components in the multiple-beam interference with Gaussian beam expansion-induced power attenuation can be modeled as (Chang and Sirkis, 1996; Yu, 2002)

$$E_{1r} = E_0 r_a e^{j\omega t}, \ E_{2r} = E_0 t_a r_b t_a' \sqrt{\alpha} e^{j(\omega t - 2kL)}, \ \text{and}$$
$$E_{3r} = E_0 t_a r_b r_a' r_b t_a' (\sqrt{\alpha})^2 e^{j(\omega t - 4kL)}, \tag{1}$$

where r_a and r_a' are the reflection coefficients of mirror a, r_b is the reflection coefficient of mirror b, and t_a and t_a' are

the transmission coefficients of mirror a. It is noted that r_a and t_a are for waves traveling from glass towards air; while r_a' and t_a' are for waves traveling from air towards glass. α is the power attenuation factor, which is defined as the fraction of the power coupled back into the single mode fiber after a roundtrip $2L$ through the FP cavity. The wave number is k, which is equal to $2\pi/\lambda$. The resultant reflected scalar E wave is given by

$$E_r = E_0 e^{j\omega t} \sqrt{R_a} \left[1 - \frac{1-R_a}{R_a} \sum_{m=1}^{\infty} (-1)^m (R_a R_b \alpha)^{m/2} e^{-2jmkL} \right],$$
$$\tag{2}$$

where $r_a = -r_a' = \sqrt{R_a}$, $t_a t_a' = T_a$, $r_b = \sqrt{R_b}$, and R and T are reflectivity and transmivity, respectively. The transfer function H_r of the F-P interferometer can be written as

$$H_r^s = \frac{E_r \cdot E_r^*}{E_i \cdot E_i^*} = A_0 - A_1 \cdot \sum_{m=1}^{\infty} (R_a R_b \alpha)^{m/2} \cdot \cos(2mkL_s),$$
$$\tag{3}$$

where

$$A_0 = R_a + \frac{(1-R_a)^2 R_b}{(1-R_a R_b)}, \ \text{and} \ A_1 = \frac{2(1-R_a-R_b+R_a R_b)}{R_a R_b - 1}.$$
$$\tag{4}$$

For a low finesse FP sensor, the transfer function can be written as

$$H_r^s = A_0 - A_1 \cdot \sqrt{R_a R_b} \alpha \cos(kL_s). \tag{5}$$

where L_s is the optical path difference of the FP interferometer and $L_s = 2L$.

Here, a path matched differential interferometery (PMDI) system is designed to demodulate the FP sensor. In this system, a read-out interferometer is path-matched to the sensing interferometer. If a read-out
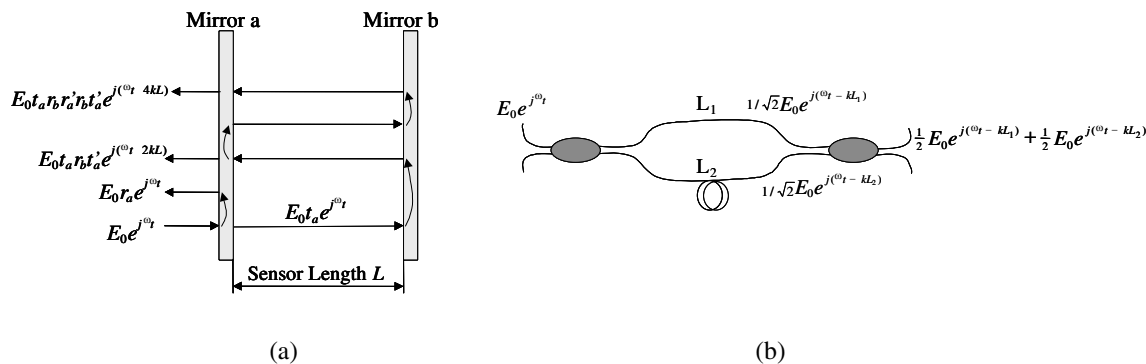
Figure 1. (a) Sensor interferometer and (b) read-out interferometer.

interferometer is a Mach-Zehnder interferometer as shown in Figure 1(b), then the associated transfer function is

$$H_t^r = \frac{E_t \cdot E_t^*}{E_i \cdot E_i^*} = \frac{1}{2}[1 + \cos k(L_2 - L_1)] = \frac{1}{2}[1 + \cos kL_r],$$
(6)

where L_r is the cavity length of the reference interferometer. When the light passes though the PMDI system, the resulting time dependent intensity function of the sensors, I_T, as detected by the photodetector is given by

$$I_T = \tfrac{1}{4} \int H_t^r H_r^s i(k) dk,$$
(7)

where H_r^s and H_t^r, which are the transfer functions of a FP sensor interferometer and a Mach-Zehnder read-out interferometer, are given by Equations (5) and (6), respectively, and $i(k)$ is the input spectrum of the broadband optical source. After carrying out the integration, Equation (7) can be written as

$$
\begin{aligned}
I_T \approx &\frac{1}{8}I_0 A_0 - \frac{1}{8}I_0 A_1 \sqrt{R_a R_b}\alpha \cos k_0 L_s e^{-(\pi L_s/L_c)^2} \\
&+ \frac{1}{8}I_0 A \cos k_0 L_r e^{-(\pi L_r/L_c)^2} - \frac{1}{16}I_0 A_1 \sqrt{R_a R_b}\alpha \\
&\left\{ \cos k_0(L_s + L_r)e^{-[\pi(L_s+L_r)/L_c]^2} \right. \\
&\left. + \cos k_0(L_s - L_r)e^{-[\pi(L_s-L_r)/L_c]^2} \right\},
\end{aligned}
$$
(8)

where L_c is the coherence length of the low coherence light source and $\Delta\lambda$ represents the half-width of the linewidth. When the system is path matched ($L_r \approx L_s$) and L_c is much smaller than L_r and L_s, interference occurs only in the $(L_s - L_r)$ component. Thus Equation (8) can be simplified to

$$I_T \approx \frac{1}{8}I_0 A_0 - \frac{1}{16}I_0 A_1 \sqrt{R_a R_b}\alpha \cos k_0(L_s - L_r).$$
(9)

Mechanical Component

Here, the sensor diaphragm is considered as a circular plate with fixed edge. A more comprehensive discussion of a plate-membrane model is provided in (Yu, 2002). This section is used to determine the relationship between the displacement of the microphone diaphragm and the pressure experienced by the diaphragm. For an isotropic circular plate of radius a and thickness h, the first natural frequency of the diaphragm can be written as

$$f = \frac{10.21}{2\pi a^2}\left[\frac{Eh^2}{12\rho(1-\nu^2)}\right]^{1/2}.$$
(10)

For forced oscillations, the governing equation is of the form

$$D\nabla^4 w + \rho h \frac{\partial^2 w}{\partial t^2} + 2\mu \frac{\partial w}{\partial t} = p(t),$$
(11)

where $p(t)$ is the dynamic sound pressure to be sensed with amplitude of p, ρ is density of the diaphragm material, ν is Poisson ratio, and $D = Eh^3/12(1 - \nu^2)$. The solution of Equation (11) can be written as

$$w(r, \theta, t) = \sum_{k=0}^{\infty} \eta_k(t)U_{3k}(r, \theta),$$
(12)

where η_k are the modal amplitudes and U_{3k} are the spatial mode components in the principal directions. Taking advantage of the orthogonality of the modes, for a harmonic loading, Equation (11) can be reduced to

$$\ddot{\eta}_k + 2\zeta_k\omega_k\dot{\eta}_k + \omega_k^2\eta_k = F_k f(t),$$
(13)

where ω_k is the natural frequency of the mode of interest and ζ_k is associated with the modal damping coefficient; the different coefficients in Equation (13) are given by

$$
\begin{aligned}
&\zeta_k = \frac{\kappa}{2\rho h\omega_k}, \qquad \kappa = \frac{\rho h\omega_k^2}{D}, \\
&F_k = \frac{1}{\rho h N_k}\int_0^a pU_{sk}(r, \theta)2\pi r dr, \text{ and} \\
&N_k = \int_0^a 2\pi r U_{sk}^2(r, \theta)dr.
\end{aligned}
$$
(14)

For harmonic excitation, the solution of Equation (13) can be written as

$$\eta_k = \Lambda_k e^{j(\omega t - \varphi_k)},$$
(15)

where the amplitude function

$$\Lambda_k = \frac{F_k}{\omega_k^2\sqrt{\left[1 - (\omega/\omega_k)^2\right]^2 + 4\zeta_k^2(\omega/\omega_k)^2}}.$$
(16)

Approximating the response given by Equation (12) in terms of a single mode, here, the first mode, the response amplitude can be written as

$$w_0(r, \theta) = \Lambda_0 U_{30}(r, \theta),$$
(17)

where

$$U_{30}(r, \theta) = A[J_0(\kappa r)I_0(\kappa a) - I_0(\kappa r)J_0(\kappa a)].$$
(18)

From Equations (14)–(18), the displacement amplitude is determined to be

$$
\begin{aligned}
&w_0(r, \theta) \\
&= \frac{2\pi pa}{\rho h\tilde{N}_0\kappa}\frac{[J_1(\kappa a)I_0(\kappa a) - I_1(\kappa a)J_0(\kappa a)][J_0(\kappa r)I_0(\kappa a) - I_0(\kappa r)J_0(\kappa a)]}{\omega_k\sqrt{\left[1 - (\omega/\omega_k)^2\right]^2 + 4\zeta_k^2(\omega/\omega_k)^2}},
\end{aligned}
$$
(19)

where

$$\tilde{N}_0 = \int_0^a 2\pi r [J_0(\kappa r)I_0(\kappa a) - I_0(\kappa r)J_0(\kappa a)]^2 dr. \quad (20)$$

For a FTFP sensor, the cavity length change is due to the deflection of the diaphragm center w_0. Hence, the optical phase change $\Delta\varphi$ is related to the sound pressure as

$$\Delta\varphi = \frac{2\pi n}{\lambda} w_0$$
$$= \frac{4\pi^2 npa}{\lambda\rho h\tilde{N}_0\kappa} \frac{[J_1(\kappa a)I_0(\kappa a) - I_1(\kappa a)J_0(\kappa a)][I_0(\kappa a) - J_0(\kappa a)]}{\omega_k\sqrt{\left[1 - (\omega/\omega_k)^2\right]^2 + 4\zeta_k^2(\omega/\omega_k)^2}},$$
$$(21)$$

where n is the reflective index of the cavity material and λ is the wavelength of light source.

SENSOR SYSTEM DESIGN

The overall sensor system is shown in Figure 2. It consists of a superluminescent light emitting diode (SLD), an integrated optical circuit (IOC) phase modulator, a 2×2 optical coupler, $1 \times N$ optical switch, FTFP sensor array, a photodetector, and a personal computer (PC) based data acquisition system. The advantage of using the optical switch to realize spatial division multiplexing (SDM) is that a larger number of sensors
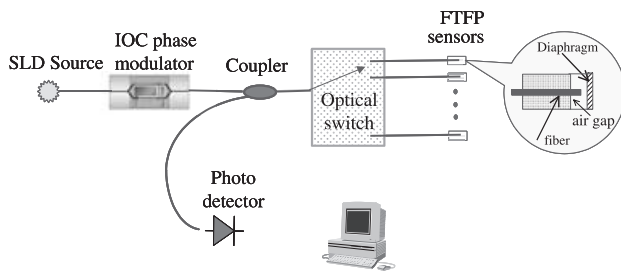
Figure 2. *Multiplexed FTFP sensor system.*
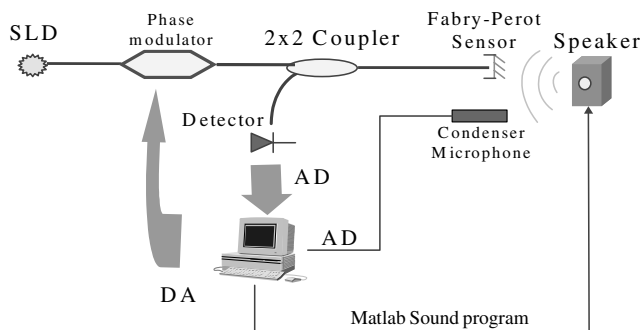
Figure 3. *Experimental arrangement to test prototype sensor system.*

can be detected by using the same base optical system (i.e., source, detectors, and modulators). Furthermore, each sensor can be designed to either sense the acoustic field at a particular location of a system or to sense a particular acoustic frequency in the system. Because of the bandwidth limitation of the optical switch, an alternative multiplexed system based on tree network topology has been demonstrated for air velocity measurements (Al-Bassyiouni et al., 2002; Yu, 2002).

High reliability connector ferrule is used to fabricate each single FTFP sensor. The diaphragm is made of Mylar film with a thickness of 40 μm and a radius of 1.75 mm. A single mode fiber is fixed in the connector ferrule and the distance between the fiber tip and the diaphragm is adjusted to 60 μm, which is half of the imbalance length in the IOC phase modulator. A sol-gel process is used to form the TiO_2 mirror on the entire cross-section of the optical fiber so that the reflectivity of the fiber tip can be increased from 4 to 16%.

EXPERIMENTAL ARRANGEMENT

The prototype sensor system based on FP technique is shown in Figure 3. The system consists of a SLD source, one 2×2 optical coupler, the FTFP sensor, an IOC phase modulator, a photodetector, and a data acquisition personal computer. The FP cavity is produced between the fiber tip and a designed diaphragm structure. The frequency response range of this diaphragm structure extends to 10 kHz. Light from the SLD is sent to the IOC phase modulator first, then via the coupler to the FTFP sensor. The reflected light from the FTFP sensor is then sent to the high-speed detector. The Mach-Zehnder interferometer inside the IOC phase modulator is path-matched to the FTFP sensor to act as a read-out interferometer. The path matching is accomplished by moving the micro-stage to adjust the distance between the fiber tip and the diaphragm. The IOC phase modulator is driven by a phase stepping program up to frequencies of 150 kHz. In the experiment, a condenser microphone (Bruel & Kjaer model # 4134) was used as reference sensor for validation. The input acoustic signal was generated by an Altec Lansing computer speaker system (Model No. ACS340). The diaphragm of the FTFP sensor is excited by using this speaker. The vibration changes the distance between the fiber tip and the diaphragm, and this displacement is related to the optical phase change. In order to detect this unknown phase change, the phase demodulation algorithm was used. The entire phase modulation and demodulation process was controlled by a PC-based digital signal processing program. A more comprehensive discussion of the phase demodulation algorithm is provided in author's previous work (Yu and Balachandran, 2001).
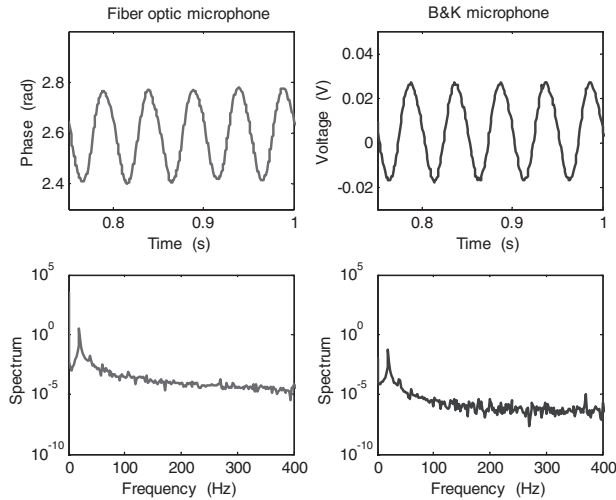
Figure 4. *Experimental results for a study performed at 20 Hz.*
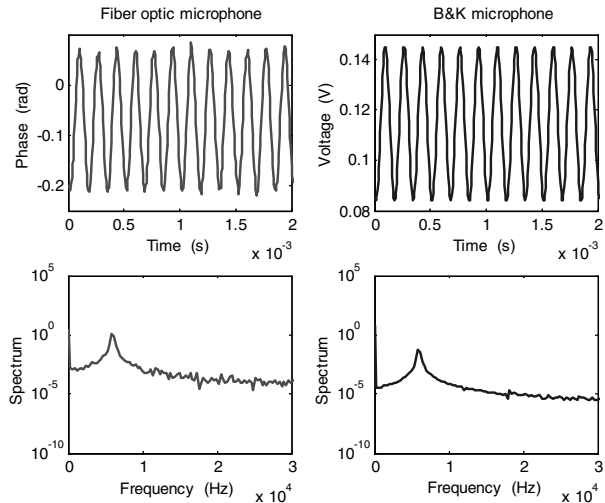
Figure 5. *Experimental results for a study performed at 6 kHz.*

Figure 6. *Sensitivity–frequency response curve for FTFP micro-phone compared with condenser microphone.*

Table 1. Resolution of FTFP sensor at different frequencies.

Frequency (Hz)	Phase Resolution (rad/$\sqrt{Hz}$)	Distance Resolution (nm/$\sqrt{Hz}$)	SPL Resolution (dB/$\sqrt{Hz}$)
20	0.00010	0.01031	38.91
100	0.00018	0.01856	43.90
400	0.00014	0.01444	41.93
2000	0.00035	0.03609	49.67
5000	0.00024	0.02475	46.41

RESULTS AND DISCUSSION

The prototype acoustic sensor is studied in a frequency range of approximately 20 Hz–6 kHz by using sinusoidal sound signals. The sensor results have been compared to the results of a Brüel & Kjær 4134 condenser microphone. Representative results from studies performed at 20 Hz and 6 kHz are shown in Figures 4 and 5. The optical sensor data compares well with the condenser microphone in both the time domain and the frequency domain.

These results are demonstrative of the applicability of the FTFP sensor system for acoustic measurements. The studies show that the system can be used in the frequency range from 20 Hz to 6 kHz. Experiments were also carried out to measure the sensitivity, linearity, signal-to-noise ratio (SNR), resolution and directivity of the FTFP microphone.

Sensitivity

The sensitivity–frequency response curve is shown in Figure 6; this curve was obtained by comparing the FTFP microphone data with condenser microphone data in the frequency range of 20 Hz–6 kHz. The sensitivity of condenser microphone is -38.06 dB (0 dB corresponds to 1.0v/Pa) as given by the manufacturer and this sensitivity is considered to be constant in the range of 20 Hz–6 kHz. It is determined that the sensitivity of FTFP sensor is 19.98 ± 0.87 dB, i.e, 0.095 rad/Pa (0 dB corresponds to 1.0 rad/Pa), which is much higher than the sensitivity of the compared condenser microphone.

Signal-to-Noise Ratio (SNR)

To determine the SNR, the noise floor needs to be defined. The noise floor is the average of the power spectrum density adjacent to the peak signal and SNR is the deference, in dB, between the peak and the noise floor. From experimental results, the SNR of FTFP microphone is determined in the frequency range of 20 Hz–6 kHz to have a mean value of 41.36 dB. It should be noted that in determining this SNR, ambient noise has not been taken into account. If the FTFP microphone is placed in an acoustic chamber without ambient noise, the SNR would be higher.
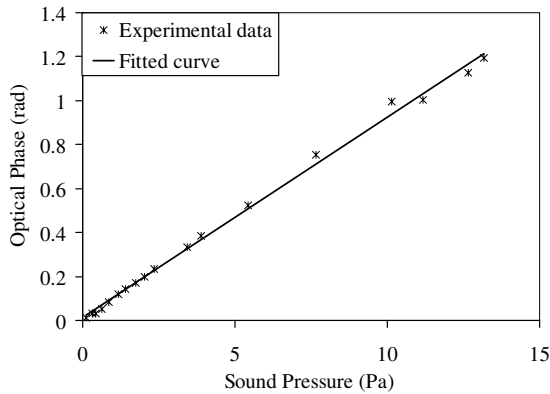
Figure 7. *FTFP microphone output vs. sound pressure.*

Further steps will aim at developing the multiplexed sensor system by using an optical switch and implementing the sensor system in acoustic control applications.

ACKNOWLEDGMENTS

Resolution

The resolution can be determined from SNR ratio by using the relation

$$\text{resolution} = (\text{signal}/10^{\text{SNR}/20}).$$

Since the signal here is optical phase at different frequencies, the unit of the resolution results in $\text{rad}/\sqrt{\text{Hz}}$. It is also possible to get distance resolution by using Equation (21) and pressure resolution by using the value of sensitivity. Some representative resolution results are presented in Table 1.

Linearity

It is assumed that the Brüel & Kjær 4134 condenser microphone has a linear response to the sound pressure to well beyond 120 dB. Comparison experiments were conducted by taking simultaneous readings from the FTFP microphone and this condenser microphone. This procedure was repeated over a range of acoustic pressures by varying the input voltage level to the loud speaker. The results, shown in Figure 7, show an excellent linear response up to 13 Pa (116 dB). Since this pressure level is the upper limit for the speaker used in the experiments, a higher sound pressure level could not be realized. A dynamic range from 50 to 116 dB was obtained. It should be noted that the true dynamic range is expected to be higher.

CONCLUDING REMARKS

A novel fiber tip Fabry-Perot (FTFP) sensor has been investigated as a possible element of a fiber optic sensor system for acoustic measurements. A PC-based pseudo-heterodyne scheme is developed in order to achieve a large sensor bandwidth. The studies were performed at frequencies in the range of 20 Hz–6 kHz. Experimental results showed that the sensor was able to sense the acoustic pressure with an acceptable accuracy and these results are in agreement with the model predictions.

REFERENCES

Al-Bassyiouni, M., Yu, M., Balachandran, B. and Oh, J. 2002. "Active Acoustics Control with Fiber Optic Sensors," In: Modeling, Signal Processing and Control, *Proceedings of SPIE*, 4693:396–405.

Balachandran, B., Sampath, A. and Park, J. 1996. "Active Control of Interior Noise in a Three-dimensional Enclosure," *Smart Materials and Structures*, 5(1):89–97.

Baldwin, C., Yu, M., Miller, C., Chen, S., Sirkis J. and Balachandran, B. 1999. "Bragg Grating Based Fabry-Perot Sensor System for Acoustic Measurements," In: International Symposium on Smart Structures and Materials, *SPIE Proceedings*, 3670:342–351.

Beard, P. C., Hurrell, A. M. and Mills, T. N. 2000. "Characterization of a Polymer Film Optical Fiber Hydrophone for Use in the Range 1 to 20 MHz: A Comparison with PVDF Needle and Membrane Hydrophones," *IEEE Transactions on Ultrasonics, Ferroelectrics, and Frequency Control*, 47(1):256–265.

Bucaro, J. A., Dardy, H. D. and Carome, E. F. 1977. "Fiber Optic Hydrophone," *Journal of Acoustical Society of America*, 62:1302–1304.

Chang, C. and Sirkis, J. S. 1996. "Multiplexed Optical Fiber Sensors using a Single Fabry-Perot Resonator for Phase Modulation," *Journal of Lightwave Technology*, 14(7):1653–1663.

Cole, J. H., Johnson, R. L. and Buta, P. G. 1977. "Fiber Optic Detection of Sound," *Journal of Acoustical Society of America*, 62:1136–1138.

Fuller, C. R., Elliott, S. J. and Nelson, P. A. 1996. *Active Control of Vibration*, Academic Press, New York.

He, G. and Cuomo, F. 1992. "The Analysis of Noises in a Fiber Optic Microphone," *Journal of Acoustical Society of America*, 92(5):2521–2526.

Koch, C. 1999. "Measurement of Ultrasonic Pressure by Heterodyne Interferometry with a Fiber-Tip Sensor," *Applied Optics*, 38(13):2812–2819.

Li, D. L. and Zhang, S. Q. 1998. "The Ring-Type All-Fiber Fabry-Perot Interferometer Hydrophone System," *Journal of the Acoustical Society of America*, 104(5):2798–2806.

Nashif, A. D., Jones, D. I. G. and Henderson, J. P. 1985. *Vibration Damping*, John Wiley &Sons, Inc., New York.

Nelson, P. A. and Elliott, S. J. 1994. *Active Control of Sound*, Academic, New York.

Takahashi, N., Yoshimura, K., Takahashi, S., and Imamura, K. 2000. "Characteristics of Fiber Bragg Grating Hydrophone," *IEIEC TRANS. ELECTRON.*, E83-C(3):275–281.

Yu, M. 2002. Fiber-Optic Sensor Systems for Acoustic Measurements, Ph.D. Dissertation, University of Maryland, College Park, MD.

Yu, M. and Balachandran, B. 2001. "Fiber Tip Based Fiber Optic Acoustic Sensors," In: *Proceeding of the 12th International Conference on Adaptive Structures and Technologies*, pp. 245–254.

Zhou, C. H., Letcher, S. V. and Shukla, A. 1995. "Fiberoptic Microphone Based on a Combination of Fabry-Perot Interferometry and Intensity Modulation," *Journal of the Acoustical Society of America*, 98(2):1042–1046.